Crystal Structure of CYP105A1 (P450SU-1) in Complex with 1α,25-Dihydroxyvitamin D_3[†,‡]

Hiroshi Sugimoto,*[,§] Raku Shinkyo,[||] Keiko Hayashi,[⊥] Sachiyo Yoneda,[||] Masato Yamada,[⊥] Masaki Kamakura,[⊥] Shin-ichi Ikushiro,[⊥] Yoshitsugu Shiro,[§] and Toshiyuki Sakaki*[,⊥]

RIKEN SPring-8 Center, Harima Institute, Sayo, Hyogo 679-5148, Japan, Division of Food Science and Biotechnology, Graduate School of Agriculture, Kyoto University, Sakyo-ku, Kyoto 606-8502, Japan, and Department of Biotechnology, Faculty of Engineering, Toyama Prefectural University, 5180 Kurokawa, Imizu, Toyama 939-0398, Japan

Received December 5, 2007; Revised Manuscript Received February 4, 2008

ABSTRACT: Vitamin D_3 (VD_3), a prohormone in mammals, plays a crucial role in the maintenance of calcium and phosphorus concentrations in serum. Activation of VD_3 requires 25-hydroxylation in the liver and 1α-hydroxylation in the kidney by cytochrome P450 (CYP) enzymes. Bacterial CYP105A1 converts VD_3 into 1α,25-dihydroxyvitamin D_3 (1α,25$(OH)_2D_3$) in two independent reactions, despite its low sequence identity with mammalian enzymes (<21% identity). The present study determined the crystal structures of a highly active mutant (R84A) of CYP105A1 from *Streptomyces griseolus* in complex and not in complex with 1α,25$(OH)_2D_3$. The compound 1α,25$(OH)_2D_3$ is positioned 11 Å from the iron atom along the I helix within the pocket. A similar binding mode is observed in the structure of the human CYP2R1−VD_3 complex, indicating a common substrate-binding mechanism for 25-hydroxylation. A comparison with the structure of wild-type CYP105A1 suggests that the loss of two hydrogen bonds in the R84A mutant increases the adaptability of the B′ and F helices, creating a transient binding site. Further mutational analysis of the active site reveals that 25- and 1α-hydroxylations share residues that participate in these reactions. These results provide the structural basis for understanding the mechanism of the two-step hydroxylation that activates VD_3.

Cytochrome P450 (CYP)[1] enzymes (*1*) form a superfamily of heme-containing monooxygenases, which catalyze remarkably diverse reactions. These enzymes are found in many bacteria and in all archaea, fungi, and higher eukaryotes (*2*). In most organisms, the primary function of these enzymes is to metabolize xenobiotic drugs and toxic chemicals. Another important role of CYP enzymes is the biosynthesis of sterols, fatty acids, and prostaglandins in mammals, insects, and plants. *Streptomyces* and other bacterial actinomyces are well-known for their ability to produce a wide variety of bioactive compounds, including antibacterial, antifungal, antitumor, and immunosuppressive agents (*3*). *Streptomyces griseolus* has two genes encoding CYPs (CYP105A1/P450SU-1 and CYP105B1/P450SU-2) that were originally identified because these CYPs metabolize various sulfonylurea herbicides (*4*). Subsequent studies revealed that CYP105A1 is capable of converting vitamin D_3 (cholecalciferol or VD_3) into its active form, 1α,25-dihydroxyvitamin D_3 (calcitriol or 1α,25$(OH)_2D_3$), by two-step hydroxylation (*5*) (Figure 1).

VD_3 acts as a prohormone in humans and other mammals (*6*). It has no hormonal activity itself but is converted to the active form by CYP enzymes. VD_3 is either consumed in food or produced from 7-dehydrocholesterol in the skin upon exposure to sunlight and is hydroxylated to 25-hydroxyvitamin D_3 (calcidiol or 25$(OH)D_3$) in the liver, where it is stored until needed. 25$(OH)D_3$ is further hydroxylated in the kidneys to the dihydroxylated metabolite, 1α,25$(OH)_2D_3$. The first hydroxylation reaction is catalyzed by mitochondrial CYP27A1 and microsomal CYP2R1 (*7*), and the second reaction is catalyzed by mitochondrial CYP27B1 (*8*) (Figure 1). Only the final product, 1α,25$(OH)_2D_3$, is hormonally active (*9–11*), mediating its biological effects by binding to the vitamin D receptor (VDR). Activation of the VDR in the intestine, bone, kidney, and parathyroid gland maintains calcium and phosphorus concentrations in the blood and preserves bone mineral content (*6*).

In addition to mammalian VD_3 hydroxylase enzymes, CYP11A1 (P450scc, cholesterol side-chain cleave enzyme), CYP11B1 (P45011*β*, steroid 11-*β*-hydroxylase), and CYP11B2 (P450aldo, steroid 18-hydroxylase), which are mitochondrial enzymes, are also involved in the biosynthesis of steroid hormones (*12–14*). To date, the X-ray crystal structures of

[†] This work was supported in part by the Ministry of Education, Culture, Sports, Science, and Technology grant (to Y.S., H.S. and T.S.) and the Sankyo Foundation of Life Sciences (to T.S.).

[‡] The atomic coordinates and structure factors (PDB codes 2ZBX, 2ZBY, and 2ZBZ) have been deposited in the Protein Data Bank (PDB), Research Collaboratory for Structural Bioinformatics, Rutgers University, New Brunswick, NJ (http://www.rcsb.org/).

* To whom correspondence should be addressed. Telephone: +81-791-58-2817. Fax: +81-791-58-2818. E-mail: sugimoto@spring8.or.jp (H.S.); Telephone: +81-766-56-7500. Fax: +81-766-56-2498. E-mail: tsakaki@pu-toyama.ac.jp (T.S.).

[§] RIKEN SPring-8 Center.

[||] Kyoto University.

[⊥] Toyama Prefectural University.

[1] Abbreviations: CYP, cytochrome P450; VD_3, vitamin D_3; 1α,25$(OH)_2D_3$, 1α,25-dihydroxyvitamin D_3; 25$(OH)D_3$, 25-hydroxyvatmin D_3; 1α$(OH)D_3$, 1α-hydroxyviamin D_3; rmsd, root-mean-square deviation; VDR, vitamin D receptor.

10.1021/bi7023767 CCC: $40.75
Published on Web 03/04/2008

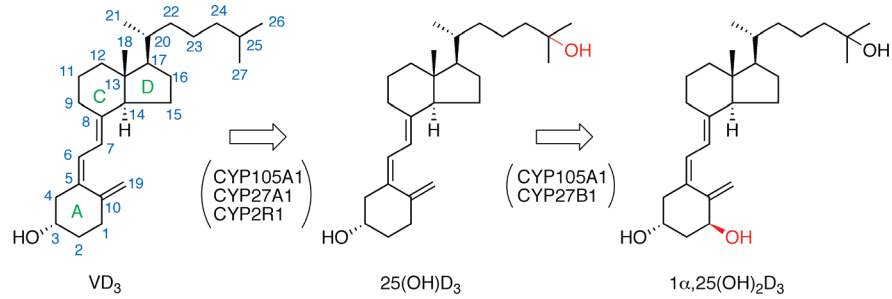

FIGURE 1: Metabolism of vitamin D_3. Liver CYP27A1 and CYP2R1 convert vitamin D_3 (VD_3) to 25-hydroxyvitamin D_3 ($25(OH)D_3$). In the kidney, CYP27B1 converts $25(OH)D_3$ to 1α,25-dihydroxyvitamin D_3 ($1\alpha,25(OH)_2D_3$). CYP105A1 can catalyze both of these reactions.

these mitochondrial CYPs have not been obtained. Homology models have been proposed for CYP27A1 and CYP27B1 (*15, 16*) based on the reported structures of the microsomal CYPs that are involved in xenobiotic or drug metabolism (CYP2C5, CYP3A4, and CYP2A6). However, because the amino acid sequence identity between mitochondrial CYP and microsomal or bacterial CYP with known structures is less than 20%, it is difficult to determine the structural basis for substrate-/inhibitor-specific recognition by enzymes. Recently, the tertiary structure of CYP2R1 in complex with VD_3 has been determined by the Structural Genomics Consortium, and its coordinates have been released (PDB code 2OJD). The structural analysis of CYP105A1, in combination with the known structure of CYP2R1, is expected to provide insight into the binding mode of steroidal substrates by mitochondrial CYPs because the regio-specific hydroxylation catalyzed by CYP105A1 is very similar to that of mammalian VD_3 hydroxylases (CYP2R1, CYP27A1, and CYP27B1) (*17*). Furthermore, in addition to the biosynthesis of antibiotics and drugs, production of the active form of VD_3 in *Streptomyces* species has been put to practical use by a food-manufacturing company (U.S. Patent 5474923). Information regarding the active site will be helpful in the design of enzymes with higher efficiencies of VD_3 activation.

This paper describes the crystal structures of wild-type CYP105A1 and the R84A mutant. The structure of the R84A mutant in complex with the final product, $1\alpha,25(OH)_2D_3$, revealed a common binding mode between bacterial and mammalian CYPs for 25-hydroxylation. Analysis of structural changes upon $1\alpha,25(OH)_2D_3$ binding and the effect of mutation on the enzyme structure and function provide the structural basis for understanding the mechanism of the two-step hydroxylation that activates VD_3.

MATERIALS AND METHODS

Material. DNA-modifying enzymes and restriction enzymes were purchased from Takara Shuzo Co. Ltd. (Kyoto, Japan). *Escherichia coli* (*E. coli*) JM109 (Takara Shuzo Co.) was used as the host strain. Ferredoxin and NADPH-ferredoxin reductase from spinach were purchased from Sigma (St. Louis, MO). VD_3, $1\alpha(OH)D_3$, $25(OH)D_3$, $1\alpha,25(OH)_2D_3$, glucose dehydrogenase, and catalase were purchased from Wako Pure Chemical Industries, Ltd. (Osaka, Japan). *S. griseolus* CYP105A1 and ferredoxin genes were kindly provided by Sumitomo Chemical Co. Ltd. (Takarazuka, Japan). NADPH was purchased from Oriental Yeast Co. Ltd. (Tokyo, Japan). Other chemicals used were of the highest quality commercially available.

Table 1: Oligonucleotides Used in PCR To Generate CYP105A1 Mutants

mutation	oligonucleotides[a]
R73A	5′-CGGCTGTCCTCCAACGCGACGGACGACAAC-3′
	5′-GTTGTCGTCCGTCGCGTTGGAGGACAGCCG-3′
R84A	5′-CCGCCACGTCACCGGCCTTCGAGGCCGTCC-3′
	5′-GGACGGCCTCGAAGGCCGGTGACGTGGCGG-3′
V88A	5′-TTCGAGGCCGCGCGGGAGAGCCCG-3′
	5′-CGGGCTCTCCCGCGCGGCCTCGAA-3′
R89A	5′-CGCTTCGAGGCCGTCGCGGAGAGCCCGCAG-3′
	5′-CTGCGGGCTCTCCGCGACGGCCTCGAAGCG-3′
L180A	5′-CGCGAGCAAGCGGGCGGTGCAGTCCACGGAC-3′
	5′-GTCCGTGGACTGCACCGCCCGCTTGCTCGCG-3′
V181A	5′-CGAGCAAGCGGCTGGCGCAGTCCACGGACG-3′
	5′-CGTCCGTGGACTGCGCCAGCCGCTTGCTCG-3′
R193A	5′-GCGCGCTCACCGCGGCGAACGACCTCGCGG-3′
	5′-CCGCGAGGTCGTTCGCCGCGGTGAGCGCGC-3′
R193Q	5′-GCGCGCTCACCGCGCAGAACGACCTCGCGG-3′
	5′-CCGCGAGGTCGTTCTGCGCGGTGAGCGCGC-3′
R193K	5′-GCGCGCTCACCGCGAAGAACGACCTCGCGG-3′
	5′-CCGCGAGGTCGTTCTTCGCGGTGAGCGCGC-3′
S236A	5′-GTGAGGAACTGATCGCCACCGCGATGCTGC-3′
	5′-GCAGCATCGCGGTGGCGATCAGTTCCTCAC-3′
I243A	5′-CGATGCTGCTCCTCGCCGCCGGCCACGAGACC-3′
	5′-GGTCTCGTGGCCGGCGGCGAGGAGCAGCATCG-3′
I293A	5′-TACCTCGCCATCGCCGACGCGGCG-3′
	5′-CGCCGCGTCGGCGATGGCGAGGTA-3′

[a] Altered base(s) for mutagenesis is underlined.

Construction of Expression Plasmids for CYP105A1 and Its Mutants. The coding region for full-length CYP105A1 with a hexahistidine tag in the C terminus was cloned into the *Nde* I and *Hind* III sites of pKSNdl that was constructed from pKK 233-3 vector (*5*). The expression plasmid was introduced into JM109 cells. Mutants were generated using a QuickChange site-directed mutagenesis kit (Stratagene) according to the instruction manual. The oligonucleotide primers that were used for mutagenesis are shown in Table 1. Correct generation of the desired mutations was confirmed by DNA sequencing.

Expression of CYP105A1 in E. coli Cells. Recombinant *E. coli* cells were grown in TB medium containing 50 μg/mL ampicillin at 37 °C. Transcription of CYP105A1 was initiated under control of the tac promoter by addition of isopropyl-thio-β-D-galactpyranoside (IPTG) at a final concentration of 1 mM when the cell density (OD_{660}) reached 0.5. δ-Aminolevulinic acid was also added at a final concentration of 0.5 mM, and the cells were then incubated with shaking at 25 °C for 46 h.

Purification of Wild-Type and Mutant CYP105A1. Cytosolic fractions prepared from each of the transformed cell cultures were applied to a Ni Sepharose column (Bio-Rad Profinity IMAC Resins) equilibrated with 20 mM Tris-HCl buffer (pH 7.4), at a flow rate of 1 mL/min. After adsorption

of wild-type or mutant CYP105A1, the column was washed with 10 column volumes of the same buffer and eluted with a linear gradient of 0–120 mM imidazole in 20 mM Tris-HCl buffer (pH 7.4). The eluted wild-type or mutant CYP105A1 was applied to a hydroxylapatite column (Econo-Pack HTC-II, Bio-Rad, Hercules, CA) equilibrated with 10 mM potassium phosphate (pH 7.4). The wild-type or mutant CYP105A1 that had passed through the hydroxylapatite column was applied to a Mono Q 5/50 GL column (GE Healthcare) equilibrated with 20 mM Tris-HCl buffer (pH 7.4). After adsorption of wild-type or mutant CYP105A1, the column was eluted with a linear gradient of 50–600 mM NaCl in 20 mM Tris-HCl buffer (pH 7.4).

Measurement of CYP105A1 Activity. Hydroxylation activity toward 1α(OH)D_3 and 25(OH)D_3 was measured in a reconstituted system containing 0.2 μM of the purified CYP105A1, 0.1 mg/mL spinach ferredoxin, 0.1 unit/mL spinach ferredoxin-NADP reductase, 1 unit/mL glucose dehydrogenase (Wako), 1% glucose, 0.1 mg/mL catalase, 1 mM NADPH, 0.5−10.0 μM of the substrate, 100 mM Tris-HCl (pH 7.4), and 1 mM ethylenediaminetetraacetic acid (EDTA) at 37 °C. The reaction was initiated by the addition of NADPH. Aliquots of the reaction mixture were collected after varying time intervals and extracted with 4 volumes of chloroform/methanol (3:1). The organic phase was recovered and dried. The resulting residue was solubilized with acetonitrile and applied to a high-performance liquid chromatography (HPLC) column under the following conditions: column, YMC-Pack ODS-AM (4 × 300 mm) (YMC Co., Tokyo, Japan); UV detection, 265 nm; flow rate, 1.0 mL/min; column temperature, 40 °C; mobile phase, a linear gradient of 70–100% aqueous acetonitrile per 15 min followed by 100% acetonitrile for 25 min for the analysis of the metabolites. When either 1α(OH)D_3 or 25(OH)$_2D_3$ is used as a substrate, a single product (1α,25(OH)$_2D_3$) is detected (*5*). The kinetic parameters, K_m and V_{max}, were calculated using nonlinear regression analysis with KaleidaGraph software (Synergy software).

Crystallization. CYP105A1 was concentrated to 0.3 mM in a buffer containing 20 mM Tris HCl (pH 7.4) using a centrifugal concentrating device. Crystals were grown using the sitting-drop vapor-diffusion method. Droplets containing 1 μL of protein and 1 μL of reservoir solution were equilibrated against 200 μL of the reservoir solution. Crystals of the wild-type enzyme in the imidazole-bound form were obtained in the reservoir solution containing 100 mM imidazole (pH 6.2), 24% PEG8000 (Sigma-Aldrich), 0.2 M NaCl, and 0.2 M Na formate. Crystals, belonging to the space group, $P2_12_12_1$ (cell dimensions of $a = 52.6$, $b = 53.8$, and $c = 140.9$ Å), with one CYP105A1 monomer in the asymmetric unit and a solvent content of 55%, formed after a few days at 10 °C. The R84A mutant was crystallized in a reservoir solution composed of 20% PEG8000, 0.1 M bis-Tris-propane (pH 6.6), 0.2 M NaCl, and 50 mM $LiNO_3$. For the preparation of the enzyme–product complex, 1α,25(OH)$_2$-D_3 was dissolved in 60% ethanol at 6 mM and then was added to the purified R84A mutant protein (0.03 mM) in 10-fold molar excess. The complex was kept on ice for 1 day, at which time the protein was concentrated to 0.3 mM. The crystal of the R84A mutant in complex with 1α,25(OH)$_2D_3$ was obtained in a reservoir solution composed of 26% PEGMME2K (Fluka), 0.1 M bis-Tris (pH 6.6), and 0.2 M NaCl. All crystals had similar unit cell dimensions and molecular packing (Table 2).

Table 2: Data Collection and Refinement Statistics

	wild type	R84A	R84A-1α,25(OH)$_2D_3$
PDB code	2ZBX	2ZBY	2ZBZ
resolution (Å)	20–1.5	20–1.6	20–1.9
high-resolution shell	1.53–1.50	1.66–1.60	1.97–1.90
space group	$P2_12_12_1$	$P2_12_12_1$	$P2_12_12_1$
unit cell dimensions (Å)	$a = 52.6$	$a = 53.4$	$a = 53.2$
	$b = 53.8$	$b = 53.6$	$b = 53.7$
	$c = 140.9$	$c = 141.3$	$c = 138.9$
wavelength (Å)	1.0	1.0	1.0
number observed	567 955	427 344	230 814
number unique	62 925	54 213	32 117
R_{merge} (%)[a,b]	3.5 (26.4)	4.0 (32.9)	5.6 (31.6)
completeness (%)[a]	97.1 (91.1)	99.4 (96.5)	100.0 (99.9)
$I/\sigma(I)$[a]	32.3 (7.4)	26.5 (5.0)	26.6 (6.8)
redundancy[a]	9.0 (8.1)	7.9 (6.5)	7.2 (6.9)
R_{work}/R_{free}[c]	0.194/0.223	0.196/0.229	0.200/0.250
number of atoms	3644	3565	3482
average B values (Å^2)			
protein	17.0	22.8	19.8
waters	27.9	34.1	29.0
other entities	13.5	14.3	22.1
rmsd bond (Å)	0.010	0.009	0.007
rmsd angle (deg)	1.31	1.26	1.10

[a] Numbers in parentheses refer to the highest resolution shell. [b] $R_{merge} = \sum_{hkl}\sum_i|I_i(hkl) - \langle I(hkl)\rangle|/\sum_{hkl}\sum_i I_i(hkl)$, where $\langle I(hkl)\rangle$ is the average intensity of the i observations. [c] $R_{work} = \sum_{hkl}||F_{obs}(hkl)| - |F_{calc}(hkl)||/\sum_{hkl}|F_{obs}(hkl)|$. R_{work} is calculated for 95% of reflections used for structure refinement. R_{free} is calculated for the remaining 5% of reflections randomly selected and excluded from refinement.

Structure Determination and Refinement. The crystals were cryo-protected by transferring them to a buffer consisting of the reservoir solution and an additional 25% glycerol. X-ray diffraction data were collected using a Quantum 210 CCD detector (ADSC) on a BL44B2 at SPring-8, Japan. All data were integrated and scaled using the HKL2000 program (*18*). Multiwavelength anomalous dispersion (MAD) (*19*) data were measured at the absorption edge of the Fe atom (Table S1 of Supporting Information). The initial phase was obtained using the autoSHARP program (*20*) and then was improved using SOLOMON (*21*). The improved phase (2.26 Å) and the high-resolution native data (1.5 Å) were used in automated model building with the ARP/wARP program (*22*). A total of 387 amino acid residues were built automatically. The heme, imidazole, and remaining residues were manually built using the graphics program, O (*23*). This model was refined using REFMAC5 (*24, 25*). The electron density of residues 87–90 located after the B helix region could not be well-defined in the wild-type enzyme. The N-terminal seven residues and the C-terminal His tag were disordered in density. The imidazole used in the crystallization buffer was bound to the heme iron as a sixth ligand. The refined structure of the wild-type enzyme was used as the starting model for the refinement of the R84A mutant and the R84A mutant−product complex. The model of the wild-type enzyme was placed directly into the unit cell of the mutant and was subjected to rigid-body refinement followed by restrained refinement. The geometric parameters for 1α,25(OH)$_2D_3$ were first obtained from coordinates of VDR (PDB code 1IE9) and then were edited using a Monomer Library Sketcher provided in CCP4i (*24*). Data collection and refinement statistics are shown in Table 2.

Molecular Docking. The structure of the R84A mutant in complex with 1α,25(OH)$_2D_3$ was used as a template for the

docking experiments. The water and 1α,25(OH)$_2$D$_3$ molecules were removed, and the remaining structure was used as the input structure. The hydrogenated protein and atomic charges of the residues were calculated using the method described in the Autodock tools package (*26*). Structures of the substrates, 25(OH)D$_3$ and 1α(OH)D$_3$, were generated by manual edition of 1α,25(OH)$_2$D$_3$. Docking experiments were performed using the Lamarckian Genetic Algorithm (LGA) method implemented in Autodock 4 (*26*). Briefly, 50 runs were carried out using the genetic algorithm. None of the side chains of the enzyme were treated as a flexible residue. Other parameters were left at the default values. Cluster analysis was performed on the docked results using a root-mean-square tolerance of 2.0 Å.

Other Calculations. Because the B′ helix of the wild-type enzyme was not modeled because of disorder and the modeling of the B′ helix of the R84A mutant without product showed weak density (Figure S1 in the Supporting Information), the structure of the product complex of the R84A mutant was compared to other CYPs using TOPP (*24*). Volumes of the distal pockets of CYP105A1, CYP167A1 (PDB code 1Q5D), and CYP107A1 (PDB code 1OXA) were calculated as probe-occupied cavity volumes from the coordinates of protein and heme using the VOIDOO program (*27*). Figures were created using PyMol software (www.pymol.org).

RESULTS

Structure Determination and Overall Fold of CYP105A1. The tertiary structure of wild-type CYP105A1 was determined using the MAD method (*19*) and was refined to a resolution of 1.5 Å. Subsequently, structures of the R84A mutant in complex and not in complex with the final product, 1α,25(OH)$_2$D$_3$, were determined at resolutions of 1.9 and 1.6 Å, respectively (Table 2). All three structures belong to the same space group with similar cell dimensions and contained one monomer in the asymmetric unit.

CYP105A1 is composed of 13 α helices (A−L) and a *β*-rich region, exhibiting the typical triangular P450 fold (Figure 2A). The topological folding and the position of the CYP105A1 heme prosthetic group are nearly identical to those of the known structures of bacterial CYP. The side and main chains comprised of 39 residues create the buried distal pocket of CYP105A1. The volume of the distal pocket of wild-type CYP105A1 is estimated to be approximately 900 Å^3, similar to the pocket volumes of P450epoK (CYP167A1) and P450eryF (CYP107A1) (802 and 881 Å^3, respectively) and 6-fold larger than van der Waals volume of VD$_3$. The active site of CYP105A1 is located in this large pocket where hydroxylation of substrates by the ferryl oxygen occurs. Similar to other CYPs, the B′ helix and F/G loop of CYP105A1 exhibit a relatively high *B* factor. In particular, the B′ helix of the wild-type enzyme is partially disordered in the absence of 1α,25(OH)$_2$D$_3$ (Figure S1 in the Supporting Information), indicating a pathway for substrate access. The superposition of CYP101 (P450cam), which is from *Pseudomonas putida* (*28*) and the most thoroughly studied bacterial CYP, with CYP105A1 results in a root-mean-square deviation (rmsd) value of 1.7 Å for the Cα atoms of 264 comparable residues, indicating overall similarity (Figure S2 in the Supporting Information). Close

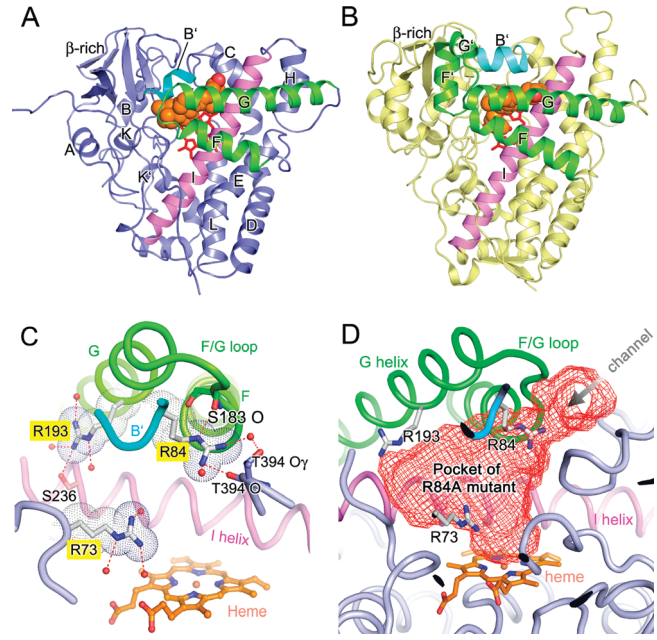

FIGURE 2: Structure of CYP105A1, compared to human CYP2R1. (A) Ribbon diagram of the CYP105A1 R84A mutant in complex with the product, as viewed from the distal side. Heme (red) is shown using a stick model. C and O atoms of 1α,25-dihydroxyvitamin D$_3$ are shown as orange and red spheres, respectively. The B′ helix, F/G region, and I helix are shown in cyan, green and purple, respectively. The helices are labeled in alphabetical order. (B) Ribbon diagram of human CYP2R1 in complex with vitamin D$_3$. The B′ helix, F/G region, and I helices are shown in the colors listed for Figure 2A. (C) Three Arg residues and surrounding water molecules in the pocket of CYP105A1 are shown using a ball-and-stick model. Note that the Arg84 side chain interacts with the carbonyl groups of Ser183 and Thr394, bridging the B′ and F helix. (D) Substrate-binding pocket of the R84A mutant in noncomplexed form (red mesh) is superimposed by three Arg residues and heme of wild-type CYP105A1.

inspection of the two enzymes (25% identity and 44% homology in their amino acid sequences) reveals conservation of CYP105A1 in individual residues and regions that play critical roles in heme-binding and dioxygen activation. The proximal ligand for the heme iron is the thiolate of Cys355 in CYP105A1 (Cys357 in CYP101) from the loop (Cys ligand loop) followed by the L helix. The I helix, the longest helix spanning the center of the molecule, contains a pair of Thr and Glu residues that are thought to play an essential role in the activation of iron-bound dioxygen (*29, 30*). Thus, CYP101 and CYP105A1 typically catalyze hydroxylation of the substrate. The conformation of the I helix of CYP105A1 shows a small bend, which is a characteristic structure of some CYPs (CYP55A1, CYP158A2, and OxyB) (*31–33*). The major structural difference between CYP105A1 and CYP101 was detected in the region between the B and C helices (B′ region) and in the short loop between the F and G helices (F/G loop). These regions show diverse amino acid sequences and fold into remarkably different conformations, with displacements of 4–5 Å after overall superposition.

The recent report on P450moxA is the first structural characterization of the CYP105 family (*34*). It shows 48% sequence identity and a rmsd value of 1.2 Å. Although the structure of P450moxA provided insights into important active-site residues, the open form of the pocket and the unexpected binding of 2-(*N*-morpholino)ethanesulfonic acid

Table 3: Comparison of 25- and 1α-Hydroxylation Activities of CYP105A1 and Mutants

	activity[a,b]	
substrate reaction	1α(OH)D_3 25-hydroxylation	25(OH)D_3 1α-hydroxylation
wild type	2.8 ± 0.3	2.1 ± 1.0
R73A	30.9 ± 8.6	20.8 ± 4.3
R84A	75.7 ± 29.2	34.5 ± 6.9
V88A	1.52 ± 0.32	0.34 ± 0.01
R89A	0.25 ± 0.05	ND
L180A	ND	ND
V181A	ND	ND
R193A	0.48 ± 0.11	0.72 ± 0.07
R193Q	0.33 ± 0.07	0.31 ± 0.06
R193K	ND	ND
S236A	4.6 ± 1.5	3.4 ± 1.0
I243A	ND	ND
I293A	5.4 ± 1.7	3.4 ± 0.5

[a] Enzymatic activities [mmol of product min^{-1} (mol of CYP)$^{-1}$] were measured using reconstituted system as described in the Materials and Methods. Results are represented as the mean ± standard deviation (SD) from three to four experiments. [b] ND = not detectable (<0.1).

(MES) from the crystallization buffer did not provide any information regarding substrate binding. Relatively higher structural similarity in the main-chain fold is detected in the following CYPs from fungi and actinomyces: CYP55A1 (P450nor), CYP107A1 (P450eryF) CYP154C1, and CYP158A2 (*31, 33, 35, 36*). These four CYPs showed 31−38% sequence identity with CYP105A1 and rmsd values of 1.4−1.5 Å for more than 325 comparable Cα atoms in the superposition with CYP105A1. In all structures, the binding pockets are large enough to accommodate a compound whose volume is larger than that of VD_3.

Active-Site Pocket of the Wild-Type Enzyme Has Three Arg Residues. Most of the amino acids that form the distal pocket are hydrophobic. However, the unique aspect of the CYP105A1 structure is that the distal pocket contains three Arg residues (Arg73, Arg84, and Arg193), the side chains of which create the distal pocket wall (Figure 2C). The distances from the iron atom are 9.3, 14.8, and 17.1 Å, respectively. The Arg73 side chain interacts with three water molecules and shows an extended conformation. Arg84 is the first residue of the B′ helix, and its side chain exhibits a high *B* factor. Its guanidium group comes in contact with two waters and carbonyl O atoms of Ser183 (in the F/G loop) and Thr394 (in the β turn). The side chain of Arg193 in the middle of the G helix is stabilized by hydrogen bonds with the OH group of Ser236 and three waters. The presence of a positively charged residue within the heme distal pocket is not rare for structures of CYP. The pocket of CYP158A2 contains Arg71 and Arg288 that interact with the carbonyls of two flaviolin molecules for the oxidative coupling reaction (*33*). The pocket of P450epoK contains Arg71 (*37*) in a position similar to that of Arg73 of CYP105A1; however, Arg71 is bound to the water rather than the substrate. The Arg residue of the fatty acid hydroxylases, CYP152A1 (P450BSβ) and CYP102A1 (P450BM-3), also play a role in substrate recognition, as the guanidium group creates a salt bridge with the carboxyl group of the fatty acid (*38, 39*). The significance of the Arg residues was examined by analyzing CYP105A1 using site-directed mutagenesis. The results (Table 3) demonstrate that, in the wild-type enzyme, Arg193 has an important role in VD_3 hydroxylation but Arg73 and Arg84 have an unfavorable role (more detail is described later).

Interaction of 1α,25(OH)$_2$D$_3$ with the R84A CYP105A1 Mutant. In the process of searching for important amino acids in the heme pocket using site-directed mutagenesis based on the structure of the wild-type enzyme, enzyme activity was increased remarkably when Arg84 was replaced with Ala. Note that Arg84 is the first residue of the B′ helix (84–90), which contains the disordered region (87–90) in the wild-type structure. The structure of this mutant (R84A) was determined in complex and not in complex with the final reaction product, 1α,25(OH)$_2$D$_3$. The omit map calculated from the data for the R84A−1α,25(OH)$_2$D$_3$ complex at 1.9 Å resolution showed unambiguous electron density for 1α,25(OH)$_2$D$_3$, which is bound along the I helix within the distal pocket (Figure 3A). The A and CD rings (in steroid notation) are bound in a narrow gap between the B′, G, and I helices. 1α,25(OH)$_2$D$_3$ is in a gently curved conformation above the heme. The distances from the iron to the two hydroxyl groups, 25-OH and 1α-OH, are 10.9 and 11.9 Å, respectively. The remaining pocket is large enough to accommodate different product conformations. The electron density for each substituent on the A ring (i.e., 1α-OH, 3β-OH, and 10-methylene groups) is well-resolved. The A ring shows an α-chair conformation with a 3β-OH group in the equatorial orientation. Figure 3B highlights the interactions between the enzyme and 1α,25(OH)$_2$D$_3$. The 10-methylene group comes in contact with Ile243 because of van der Waals interaction. The 3β-OH group on the C3 atom is hydrogen-bonded to the side chain of Arg193 of the G helix. The 1α-OH group does not interact with protein residues but with a water molecule (Wat-188 in Figure 3A). The C6–C7 double bond is sandwiched by Val88 and Leu180 and exhibits a torsion angle (C5–C6–C7–C8) of 176°. The electron density of the CD ring of the steroid core is also excellent. Ala84 is located at 4.4 Å from the C12 atom of the C ring. The line of hydrophobic amino acids (Val181, Leu180, Ile243, and Met239) comes in contact with one side of the plane of the CD rings. On the opposite side of the ring, the methyl C18 on the C ring points toward Phe85 in close van der Waals' contact. Arg73 is located 6 Å from the C ring but does not come in contact with the ring. The 17β aliphatic side chain is located in the hydrophobic cavity comprised of Phe85 and Ile293. However, the terminal groups of 25-OH, C26 methyl and C27 methyl, are disordered, and the shape of the density indicates the presence of a minor conformation for the tail after C24. Structural refinement resulted in convergence of the positions of the 25-OH and the C26 methyl group, such that they interact with the carbonyl O of Ile293 and the Ile293 side chain, respectively (Figure 3B). The conformational flexibility of Ile293 and its less specific interaction with the tail of the aliphatic side chain of 1α,25(OH)$_2$D$_3$ may explain the substrate tolerance toward vitamin D_2 (*5*), which contains a C22–C23 double bond.

Superposition between the complexed and noncomplexed structures of the R84A mutant results in rmsd of 0.4 Å, implying overall conformational similarity. However, binding of 1α,25(OH)$_2$D$_3$ apparently induces structural differences in three regions. The first difference is the conformational change and the better-ordered B′ helix of the complex (Figure S1 in the Supporting Information). Second, the loop region of residues 292–294 followed by the K helix exhibits a

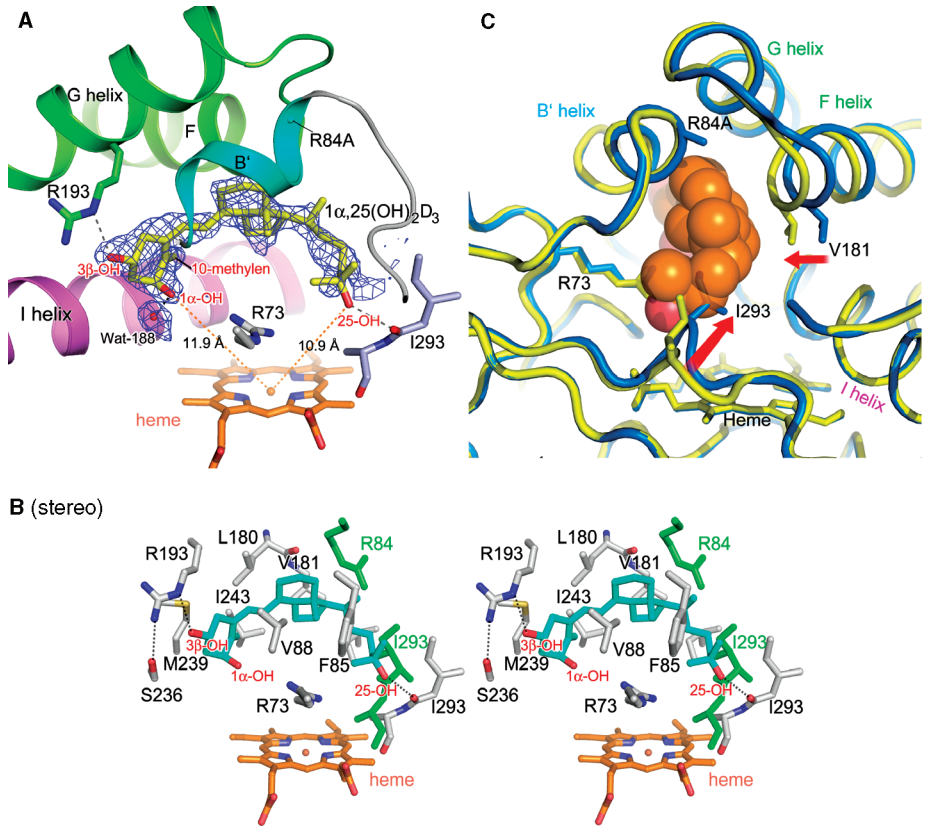

FIGURE 3: 1α,25(OH)$_2$D$_3$-Binding site of the CYP105A1 R84A mutant. (A) Electron-density map ($F_o - F_c$) for 1 α,25(OH)$_2$D$_3$ was calculated as omit maps and contoured at the 2.2σ level (blue mesh). The main chain of the protein is shown using a ribbon model. Arg73 and Arg193 and Ile293 and Ala294 are shown as stick models. The heme and 1α,25(OH)$_2$D$_3$ are shown using orange and yellow stick models, respectively. The nitrogen and oxygen atoms are shown in blue and red, respectively. The helices are indicated by the colors listed in parts A and C of Figure 2. (B) Stereo diagram of the amino acid residues involved in the interaction with 1α,25(OH)$_2$D$_3$. Amino acid residues involved in 1α,25(OH)$_2$D$_3$ recognition are shown in stick models. The carbon atoms of the protein residues of the R84A mutant, heme, and 1α,25(OH)$_2$D$_3$ are shown in white, orange, and cyan, respectively. The side chain of Arg84 and the Ile293 and Ala294 regions of the wild-type enzyme (noncomplexed form) are superimposed as a green stick model. Hydrogen bonds are shown as dotted lines between the donor and acceptor. (C) Conformational change upon 1α,25(OH)$_2$D$_3$ binding is shown. Main-chain trace of the 1α,25(OH)$_2$D$_3$-complexed form (yellow) and noncomplexed form (light blue) are superimposed. The heme, Arg73, Ala84, Val181, and Ile293 are shown using a stick model. The bound 1α,25(OH)$_2$D$_3$ is represented by the spheres.

conformational change with a 3.1 Å shift to prevent steric hindrance of 1α,25(OH)$_2$D$_3$ (Figure 3C). Third, the region of Leu180 and Val181 at the end of the F helix also shifts by 2.8 Å toward 1α,25(OH)$_2$D$_3$, more tightly packing the B′ and F helices (Figure 3C). Additionally, the presence of the compound slightly displaces the G helix containing Arg193 by 0.3–0.7 Å to establish a polar interaction of 3β-OH with Arg193, while no conformational changes are apparent in the Arg193 side chain.

Analysis of Site-Directed Mutagenesis Indicates a Common Recognition Site for Both Reactions. The time course of products in the metabolism of VD$_3$ by the enzyme shows that the dihydroxylated product, 1α,25(OH)$_2$D$_3$, is detected after the accumulation of monohydroxylated product (not shown), suggesting that the monohydroxylated product must exit the active site and re-enter for a second hydroxylation. When either 1α(OH)D$_3$ or 25(OH)D$_3$ was added as a substrate in the reaction mixture containing either CYP105A1 or its active mutant, 1α,25(OH)$_2$D$_3$ was detected as a single metabolite. It is noted that 1α(OH)D$_3$ is a better substrate for CYP105A1 than VD$_3$, as described previously (*5*). Although 1α(OH)D$_3$ is not a biological substrate, it is used clinically for the treatment of osteoporosis. In the liver, 1α(OH)D$_3$ is converted to 1α,25(OH)$_2$D$_3$ by CYP27A1 and CYP2R1. In our assay, 1α(OH)D$_3$ was used as the substrate in the measurements of 25-hydroxylation activity and 25(OH)D$_3$ was used for 1α-hydroxylation activity for conversion to a single dihydroxylated product. Table 3 shows the comparison of hydroxylation activities of wild type and various mutants. The wild-type enzyme exhibits 25-hydroxylation of 1α(OH)D$_3$ that is higher than the 1α-hydroxylation of 25(OH)D$_3$. Mutation of the hydrophobic amino acids (V88A, L180A, and V181A) that are involved in the interaction with 1α,25(OH)$_2$D$_3$ result in decreased or undetectable activities for both substrates. Slightly increased activities of the I293A mutants indicate the significance of the flexible loop containing this residue. Decreased activities of R193A, R193Q, and R193K mutants suggest that the interaction between the Arg193 side chain and the 3-OH group of the substrate is closely involved in the activity of both 25-hydroxylation and 1α-hydroxylation.

Remarkably, the R73A and R84A mutants demonstrate an increase in both activities. As shown in Table 4, kinetic analysis reveals that V_{max} of the R84A mutant for 25-hydroxylation increased 32-fold. Nonetheless, the K_m (9.8 μM) is very similar to that of the wild-type enzyme (9.4 μM). The V_{max} for 1α-hydroxylation by R84A increases 7-fold, and the K_m decreases 0.5-fold. Mutation of R73A significantly increases V_{max} and decreases K_m for both reactions. The structural explanation for the hyperactivity

Table 4: Comparison of 1α(OH)D_3 and 25(OH)D_3 Hydroxylation Kinetics for CYP105A1 and Its Mutants

reaction	25-hydroxylation			1α-hydroxylation		
substrate	1α(OH)D_3			25 (OH)D_3		
	K_m (μM)	V_{max} [mmol min^{-1} (mol of CYP)$^{-1}$]	V_{max}/K_m	K_m (μM)	V_{max} [mmol min^{-1} (mol of CYP)$^{-1}$]	V_{max}/K_m
wild type	9.4 ± 5.7	8.4 ± 2.9	0.9	5.0 ± 4.6	3.8 ± 1.6	0.8
R84A	9.8 ± 1.6	267.8 ± 24.4	27.3	2.5 ± 1.7	26.1 ± 2.1	10.4
R73A	6.5 ± 1.5	133.1 ± 16.4	20.5	3.2 ± 0.9	30.0 ± 3.4	9.4

of the R73A mutant is that contact with the hydrophobic CD ring of the substrate is unfavorable to the wild-type enzyme.

Interestingly, all mutants in Table 3 clearly show that the two reactions are similarly affected by the mutation. Furthermore, none of the mutants exhibits a change in substrate preference or regio-specificity (data not shown). Because the hydroxylation positions (C1 and C25) in the chemical structure of VD_3 are >10 Å apart, the orientations of the substrate within the pocket are expected to differ significantly between the two reactions. If the contact residues for the substrate of the 25-hydroxylation, i.e., 1α(OH)D_3, were different from the contact residues for 25(OH)D_3 in 1α-hydroxylation, then the effects of mutation on the two activities should be independent. Therefore, the result of mutation analysis of CYP105A1 indicates that common residues are involved in the substrate recognition that is required for 25-hydroxylation and 1α-hydroxylation.

Effect of the R84A Mutation on the Enzyme Structure and Function. The hydrophobic interaction between the Ala84 of R84A mutant and 1α,25$(OH)_2D_3$ in the crystal structure indicates that Arg is one of the most important residues controlling the substrate position. Previous research suggests that the B′ and F helices of the other CYPs are important for the control of substrate specificity (*40*). However, the cause of the increased activity resulting from the R84A mutation would be somewhat different, because the K_m of the R84A mutant in 25-hydroxylation of 1α(OH)D_3 is very similar to that of the wild-type enzyme. Structural superposition between the wild type and R84A mutant (noncomplexed forms) gives a rmsd value of 0.4 Å for 394 visible Cα atoms, indicating a small effect of the mutation on the overall structure. However, a slightly open structure of the F helix and the loss of the bulky side chain of Arg84 in the B′ helix create a narrow channel, connecting the active site to the solvent region in the R84A mutant (Figure 2D). The looser packing of the F helix can be explained by the loss of the interaction between the Arg84 side chain and the O on Ser183 (F/G loop) (Figure 2C). Because the channel is too narrow for the substrate to pass through, one structural explanation for the increased activity of the R84A mutant is that the mutation increases the adaptability of the hydrophobic residues (Leu180 and Val181) of the F helix, positioning the substrate in a more reactive site. Alternatively, the looser packing of the F helix may increase the product-release rate. It is also possible that more rapid escape of the product from the reaction site to the observed 1α,25$(OH)_2D_3$-binding site might increase the product-release rate. Overall, these results demonstrate the importance of the mobility of the F helix and suggest a gating role in enzyme function for Arg84 of the B′ helix. The channel described here is consistent with one of the major substrate-access and product-release pathways proposed for other CYPs (*41*). In any case, transient-state kinetic analysis is necessary to determine the rate-limiting step and evaluate these hypotheses.

Docking Calculations. As mentioned above, the large pocket is large enough to accommodate various conformations of either the substrate or the product. Studies of CYP101 (*42*) indicate that the substrate moves to a position suitable for the reaction upon complex formation with its electron-transfer partner. To examine the possible orientation and conformation of the substrate within the pocket, docking calculations were performed using the AutoDock program (*26*). Figure 4A shows the docking model of 1α(OH)D_3 for 25-hydroxylation in the R84A mutant that was used as a template. The results show that 1α(OH)D_3 binding in closer proximity to the heme within the pocket is energetically permissible. When its orientation is compared to that of

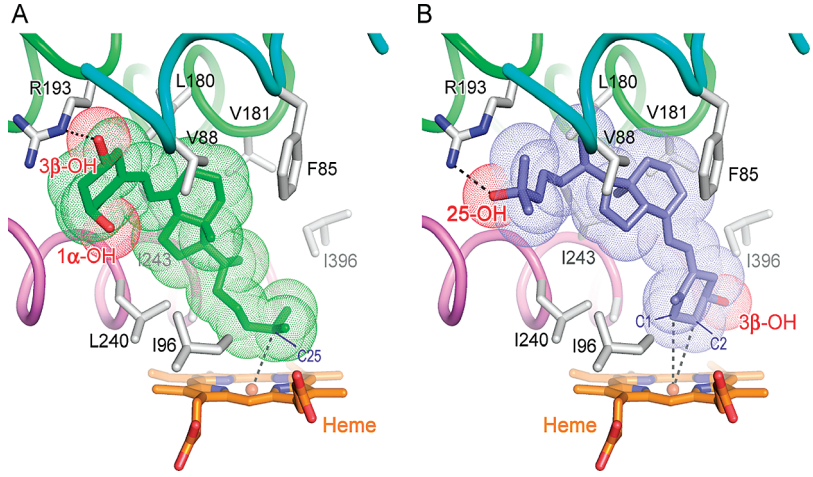

FIGURE 4: Results of docking calculations. (A) Docking model of 1α(OH)D_3 as a substrate for 25-hydroxylation. (B) Docking model of 25(OH)D_3 as a substrate for 1α-hydroxylation. The helices (B′, F, G, and I) are shown in the colors as listed for parts A and C of Figure 2 and Figure 3A.

1α,25(OH)$_2$D$_3$ in the crystal structure, steroid rings are rotated ~45° along the A ring that is anchored by the hydrogen bond between the 3β-OH group and Arg193. The distance from the C25 atom to iron is suitable for hydroxylation (4 Å). Whereas the hydrophobic CD ring interacts with Ile243 of the I helix, it retains its hydrophobic interactions with Val88, Leu180, and Val181, which is consistent with the decreased activity, as shown in Table 3. The Arg73 also close to the hydrophobic CD ring of the model explains the increased activity of the R73A mutant. Losing the positively charged Arg73 may stabilize substrate binding in the reaction site. The 17β aliphatic side-chain conformation, which was set to be flexible in the calculation, is restrained by several hydrophobic amino acids (Ile96, Leu240, Ala244, and Ile396) and presents the C25 position in proximity to the heme iron.

The docking site of 25(OH)D$_3$ is very similar to that of 1α(OH)D$_3$ (Figure 4B). These substrates are recognized by common residues, which is consistent with the results of site-directed mutagenesis. The docking model of 25(OH)D$_3$ is anchored by a hydrogen bond between the 25-OH group and Arg193. The A ring is placed closest to the heme. However, contrary to our expectations, it is the C2 position rather than the C1 position that is closer to the heme iron. Apparently, it is difficult for the C1 atom of 25(OH)D$_3$ to closely access heme iron because of the steric hindrance between the steroid rings and the amino acids around the heme. In addition, the torsion angle between A and C rings is restrained by the planarity of the triene moiety (C19−C10−C5−C6−C7−C8). It seems likely that either additional local conformational changes in the hydrophobic amino acids in the substrate-binding pocket or other larger scale conformational changes are required for 1α-hydroxylation. Alternatively, restraints by surrounding amino acids might cause a distortion in the triene moiety of the substrate, thereby bringing the C1α position into proximity with the heme iron. These structural characteristics might reflect the lower activity of 1α-hydroxylation compared to the 25-hydroxylation in the wild-type and mutant enzymes tested in the present study.

Location and Orientation of 1α,25(OH)$_2$D$_3$ Are Similar to Those of VD$_3$ in the Structure of CYP2R1. Recently, Strushkevich et al. analyzed the X-ray crystal structure of human microsomal VD$_3$ 25-hydroxylase CYP2R1 in complex with the substrate, VD$_3$ (PDB code 2OJD), thus revealing the specific interaction between the enzyme and VD$_3$ required for 25-hydroxylation. As illustrated in parts A and B of Figure 2, a comparison of the main-chain folds shows a large difference in the F/G region, where CYP2R1 contains extra helices F′ and G′ as do other microsomal CYPs. Neither F′ nor G′ helices of CYP2R1 has direct contact with VD3, but both appear to be involved in the formation of the substrate channel in the bilayer lipid membrane. The VD$_3$-binding site of CYP2R1 shows some similarities to the 1α,25(OH)$_2$D$_3$-binding site of CYP105A1 (Figure 5). In CYP2R1, the A ring of VD$_3$ is bound in the space between the B′, G, and I helices, mainly by hydrophobic interaction. Only one polar interaction of VD$_3$ involves the 3β-OH group that is hydrogen-bonded to the O on Ala250 in the G helix of CYP2R1. Note that Ala250 corresponds, in both sequence and structural alignment, to Arg193 of CYP105A1. The C25 atom of VD$_3$ in the CYP2R1−VD$_3$ complex is located 6.4 Å from the heme iron, which is closer but estimated to be out of reach of the ferryl oxygen. These similarities suggest a common VD$_3$-binding mode in bacterial CYP105A1 and human CYP2R1 for 25-hydroxylation.

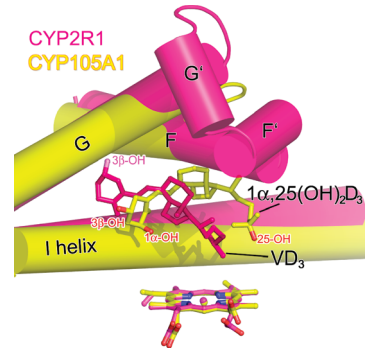

FIGURE 5: Active site of CYP105A1 and CYP2R1. Superposition of the active site of CYP105A1 (yelllow) and CYP2R1 (red). 1α,25(OH)$_2$D$_3$ in complex with the CYP105A1 complex and VD$_3$ in complex with CYP2R1 have similar orientations with a rmsd value of 2.2 Å for comparable atoms. Helices are represented by cylinders. In contrast to the short loop connecting the F and G helices in CYP105A1, CYP2R1 has two extra helices (F′ and G′).

DISCUSSION

Design of Highly Active Mutants. The experiments described in this paper demonstrate that substitution of Arg73 or Arg84 by site-directed mutagenesis greatly enhances both 1α- and 25-hydroxylation activities and that Arg193 is important for hydroxlyation reactions. CYP105A1 and its isoform, CYP105B1 (P450SU-2: 43% sequence identity; 61% homology), were originally identified for their ability to metabolize sulfonylurea herbicides (*4*). Therefore, it has been speculated that these enzymes play a role in xenobiotic metabolism in *S. griseolus*. Because none of the three Arg residues (73, 84, and 193) described above is conserved between CYP105A1 and CYP105B1, they do not appear to have an essential role in sulfonylurea metabolism, even though it is a water-soluble substrate. Members of the CYP105 family have broad substrate specificity and, thus, the potential for producing useful chemicals in bioconversion systems. CYP105A3 (P450sca-2) from *Streptomyces carbophilus* is used for the biosyntheis of pravastatin, an enzyme inhibitor of cholesterol biosynthesis (*43*). Application of CYP105D1 (P450soy) to bioremediation is indicated because CYP105D1 degrades a diverse array of complex agrochemicals and environmental pollutants (*44*). Because the conversion of VD$_3$ to 1α,25(OH)$_2$D$_3$ by wild-type CYP105A1 is too inefficient to be used on an industrial scale, our successful strategy for increasing enzyme activity by site-directed mutagenesis will guide future enhancement of enzyme activity for practical applications. The structural information presented here will also be helpful for designing other CYPs that can be used for the synthesis of useful agents, such as antibiotics or antitumor drugs.

Role of the Primary Binding Site. The distances (~11 Å) from the hydroxylation site (C25 or C1) to iron in the R84A mutant in complex with 1α,25(OH)$_2$D$_3$ appears to be too far to simulate the reactive structure of the enzyme–substrate complex for hydroxylation (Figure 3). Nonetheless, a comparison to the structure of the CYP2R1−VD$_3$ complex suggests that the observed orientation of 1α,25(OH)$_2$D$_3$ appears to reflect the orientation required for the 25-

hydroxylation reaction. Therefore, it is possible that the 1α,25(OH)$_2$D$_3$-binding site in the present structure serves as a transient binding site for both the substrate and the reaction product, as a result of the increased adaptability of the active site. When the substrates for 25-hydroxylation (i.e., 1α(OH)D$_3$ or VD$_3$) bind to this transient site, its position and conformation might be similar to that observed for 1α,25(OH)$_2$D$_3$, because the 1α-OH group of the product is free from any enzyme contact and the tail of the aliphatic side chain is not tightly bound to the enzyme. This scenario is reminiscent of the primary binding site of *S*-warfarin in the CYP2C9 complex (*45*). As proposed for CYP2C9, the substrate might first be transiently bound to the putative primary binding site and then move to a position that is suitable for metabolism. Simultaneous binding of more than one substrate molecule is not possible, because CYP105A1 and its mutants do not show cooperativity but instead are governed by Michaelis–Menten kinetics. Some crystal structures of prokaryotic CYPs in complex with a substrate have shown a closer location of the substrate to heme iron. The distance between the hydroxylated carbon atom and the heme iron in CYP101, CYP167A1, and CYP107A1 are 4.5, 4.7, and 4.8 Å, respectively (*35, 37, 46*). However, in P450 BM3 (CYP102), the bound substrate (palmitoleic acid) is positioned more than 7 Å from the heme iron (*38*). Nuclear magnetic resonance (NMR) paramagnetic relaxation studies are in good agreement with the crystal structure of CYP102 and show that the substrate moves several angstroms closer to the iron when the heme is reduced with dithionite (*47, 48*). NMR studies on CYP101 also suggest the substrate (camphor) moves to the heme iron by 0.15–0.7 Å upon binding of the electron-donor putidaredoxin (*42*). P450 PikC (CYP107L1) catalyzes monohydroxylation at either C10 or C12 of the macrolactone ring (YC-17) to yield methymycin and neomethymycin, respectively. These carbon atoms are positioned at 5.3–7.4 Å from the heme iron (*49*). These studies indicate that, assuming substrate binding to the primary recognition site of CYP105A1, interactions of CYP105A1 with the electron-transfer partner may allow for substrate molecules to move to a position that is suitable for metabolism.

Implications for Mammalian Vitamin D Hydroxylase. Recent findings show that the microsomal CYPs are bound to the endoplasmic reticulum by only one transmembrane peptide located at the N-terminal end and that a large cytoplasmic domain may have additional peripheral membrane contacts in the vicinity of the β-rich region (*2*). In contrast, in the mature form, mitochondrial CYPs lack a hydrophobic N terminus (*50*) and, thus, may differ significantly from the microsomal CYPs. Therefore, it is most difficult to predict either the substrate-binding mode and pathway of substrate entry or the product release in mitochondrial CYPs based on known CYP structures. However, a similar orientation of 1α,25(OH)$_2$D$_3$ in CYP105A1 and VD$_3$ in CYP2R1 (Figure 5) suggests a general mechanism for the recognition of vitamin D by the CYP family, including mitochondrial CYP27A1, because the substrate preference and regio-specificity of CYP27A1 closely resemble those of CYP105A1 (*5*). Our mutation analysis combined with the docking calculation agrees with the two modes of substrate recognition in an enzyme. It is likely that the ability of CYP105A1 to bind the relatively large substrate VD$_3$ (i.e., M_r = 384.6) in such a mechanism is one of the few examples among CYPs with functions that have been characterized. Similarly, two modes of substrate binding have been indicated for rat CYP2C3 in 16α- and 6β-hydroxylation of progesterone (M_r = 314.5) (*51*). The 25- and 1α-hydroxylation activities can be detected for CYP27A1 and CYP27B1 when the recombinant enzymes with reconstituted systems are used for *in vitro* measurement (*52*).

In summary, structural analysis of CYP105A1 revealed that the location and orientation of 1α,25(OH)$_2$D$_3$ observed in a R84A mutant with high activity are similar to that of VD$_3$ in human CYP2R1, suggesting a common substrate-binding mode for 25-hydroxylation. R84A shows a 32-fold increase in 25-hydroxylation activity compared to the wild-type enzyme. A plausible explanation for this effect of the R84A mutant is that the loss of the interaction with the Arg84 side chain in B′ helix opens a direct channel to the active site and increases the adaptability of hydrophobic amino acids. Mutational analysis revealed that the 25- and 1α-hydroxylations have several important residues in common. Substrate-docking studies have also indicated that 1α(OH)D$_3$ and 25(OH)D$_3$ bind to the common site in two distinct orientations that present opposite ends of the sterol to the heme iron. This study provides the structural basis of activation of VD$_3$ by CYP105A1 and proposes an underlying mechanism for two-step hydroxylation. In addition, the results will guide the design of CYPs that can be used for the production of hormonally active forms of VD$_3$.

ACKNOWLEDGMENT

We thank Taiji Matsu, Takaaki Hikima, Go Ueno, and Masaki Yamamoto for their assistance with the RIKEN beam line at SPring-8. The authors thank Shingo Nagano for the productive discussion and reading the manuscript.

SUPPORTING INFORMATION AVAILABLE

A table giving the statistics of X-ray data collection and MAD phasing for the native crystal (Table S1), a figure showing the electron density of the B′ helix (Figure S1), and a figure showing the structural superposition of CYP105A1 and CYP101 (Figure S2). This material is available free of charge via the Internet at http://pubs.acs.org.

REFERENCES

1. Omura, T., and Sato, R. (1962) A new cytochrome in liver microsomes. *J. Biol. Chem. 237*, 1375–1376.
2. Ortiz de Montellano, P. R. (2005) *Cytochrome P450: Structure, Mechanism, and Biochemistry*, 3rd ed., Kluwer Academic/Plenum Publishers, New York.
3. Demain, A. L., and Fang, A. (2000) The natural functions of secondary metabolites. *Adv. Biochem. Eng. Biotechnol. 69*, 1–39.
4. Omer, C. A., Lenstra, R., Litle, P. J., Dean, C., Tepperman, J. M., Leto, K. J., Romesser, J. A., and O'Keefe, D. P. (1990) Genes for two herbicide-inducible cytochromes P-450 from *Streptomyces griseolus*. *J. Bacteriol. 172*, 3335–3345.
5. Sawada, N., Sakaki, T., Yoneda, S., Kusudo, T., Shinkyo, R., Ohta, M., and Inouye, K. (2004) Conversion of vitamin D$_3$ to 1α,25-dihydroxyvitamin D$_3$ by *Streptomyces griseolus* cytochrome P450SU-1. *Biochem. Biophys. Res. Commun. 320*, 156–164.
6. Jones, G., Strugnell, S. A., and DeLuca, H. F. (1998) Current understanding of the molecular actions of vitamin D. *Physiol. Rev. 78*, 1193–1231.
7. Cheng, J. B., Levine, M. A., Bell, N. H., Mangelsdorf, D. J., and Russell, D. W. (2004) Genetic evidence that the human CYP2R1

enzyme is a key vitamin D 25-hydroxylase. *Proc. Natl. Acad. Sci. U.S.A. 101*, 7711–7715.
8. Takeyama, K., Kitanaka, S., Sato, T., Kobori, M., Yanagisawa, J., and Kato, S. (1997) 25-Hydroxyvitamin D_3 1α-hydroxylase and vitamin D synthesis. *Science 277*, 1827–1830.
9. Holick, M. F., Schnoes, H. K., and DeLuca, H. F. (1971) Identification of 1,25-dihydroxycholecalciferol, a form of vitamin D_3 metabolically active in the intestine. *Proc. Natl. Acad. Sci. U.S.A. 68*, 803–804.
10. Lawson, D. E., Fraser, D. R., Kodicek, E., Morris, H. R., and Williams, D. H. (1971) Identification of 1,25-dihydroxycholecalciferol, a new kidney hormone controlling calcium metabolism. *Nature 230*, 228–230.
11. Norman, A. W., Myrtle, J. F., Midgett, R. J., Nowicki, H. G., Williams, V., and Popjak, G. (1971) 1,25-dihydroxycholecalciferol: Identification of the proposed active form of vitamin D_3 in the intestine. *Science 173*, 51–54.
12. Bureik, M., Lisurek, M., and Bernhardt, R. (2002) The human steroid hydroxylases CYP1B1 and CYP11B2. *Biol. Chem. 383*, 1537–1551.
13. Kawamoto, T., Mitsuuchi, Y., Toda, K., Yokoyama, Y., Miyahara, K., Miura, S., Ohnishi, T., Ichikawa, Y., Nakao, K., Imura, H., Ulick, S., and Shizuta, Y. (1992) Role of steroid 11 β-hydroxylase and steroid 18-hydroxylase in the biosynthesis of glucocorticoids and mineralocorticoids in humans. *Proc. Natl. Acad. Sci. U.S.A. 89*, 1458–1462.
14. Nebert, D. W., and Russell, D. W. (2002) Clinical importance of the cytochromes P450. *Lancet 360*, 1155–1162.
15. Prosser, D. E., Guo, Y., Jia, Z., and Jones, G. (2006) Structural motif-based homology modeling of CYP27A1 and site-directed mutational analyses affecting vitamin D hydroxylation. *Biophys. J. 90*, 3389–3409.
16. Yamamoto, K., Masuno, H., Sawada, N., Sakaki, T., Inouye, K., Ishiguro, M., and Yamada, S. (2004) Homology modeling of human 25-hydroxyvitamin D3 1α-hydroxylase (CYP27B1) based on the crystal structure of rabbit CYP2C5. *J. Steroid Biochem. Mol. Biol. 89–90*, 167–171.
17. Sawada, N., Sakaki, T., Ohta, M., and Inouye, K. (2000) Metabolism of vitamin D_3 by human CYP27A1. *Biochem. Biophys. Res. Commun. 273*, 977–984.
18. Otwinowski, Z., and Minor, W. (1997) Processing of X-ray diffraction data collected in oscillation mode. *Methods Enzymol. 276*, 307–326.
19. Hendrickson, W. A. (1991) Determination of macromolecular structures from anomalous diffraction of synchrotron radiation. *Science 254*, 51–58.
20. de La Fortelle, E., and Bricogne, G. (1997) Maximum-likelihood heavy-atom parameter refinement for multiple isomorphous replacement and multiwavelength anomalous diffraction methods. *Methods Enzymol. 276*, 472–494.
21. Abrahams, J. P., and Leslie, A. G. (1996) Methods used in the structure determination of bovine mitochondrial F_1 ATPase. *Acta Crystallogr., Sect. D: Biol. Crystallogr. 52*, 30–42.
22. Morris, R. J., Perrakis, A., and Lamzin, V. S. (2003) ARP/wARP and automatic interpretation of protein electron density maps. *Methods Enzymol. 374*, 229–244.
23. Jones, T. A., Zou, J. Y., Cowan, S. W., and Kjeldgaard, M. (1991) Improved methods for building protein models in electron density maps and the location of errors in these models. *Acta Crystallogr., Sect. A: Found. Crystallogr. 47*, 110–119.
24. Collaborative Computational Project, Number 4. (1994) The CCP4 suite: Programs for protein crystallography, *Acta Crystallogr., Sect. D: Biol. Crystallogr. 50*, 760–763.
25. Murshudov, G. N., Vagin, A. A., and Dodson, E. J. (1997) Refinement of macromolecular structures by the maximum-likelihood method. *Acta Crystallogr., Sect. D: Biol. Crystallogr. 53*, 240–255.
26. Morris, G. M., Goodsell, D. S., Halliday, R. S., Huey, R., Hart, W. E., Belew, R. K., and Olson, A. J. (1998) Automated docking using a Lamarckian genetic algorithm and an empirical binding free energy function. *J. Comput. Chem. 19*, 1639–1662.
27. Kleywegt, G. J., and Jones, T. A. (1994) Detection, delineation, measurement and display of cavities in macromolecular structures. *Acta Crystallogr., Sect. D: Biol. Crystallogr. 50*, 178–185.
28. Poulos, T. L., Finzel, B. C., Gunsalus, I. C., Wagner, G. C., and Kraut, J. (1985) The 2.6-Å crystal structure of *Pseudomonas putida* cytochrome P-450. *J. Biol. Chem. 260*, 16122–16130.
29. Gerber, N. C., and Sligar, S. G. (1994) A role for Asp-251 in cytochrome P-450cam oxygen activation. *J. Biol. Chem. 269*, 4260–4266.
30. Imai, M., Shimada, H., Watanabe, Y., Matsushima-Hibiya, Y., Makino, R., Koga, H., Horiuchi, T., and Ishimura, Y. (1989) Uncoupling of the cytochrome P-450cam monooxygenase reaction by a single mutation, threonine-252 to alanine or valine: Possible role of the hydroxy amino acid in oxygen activation. *Proc. Natl. Acad. Sci. U.S.A. 86*, 7823–7827.
31. Park, S. Y., Shimizu, H., Adachi, S., Nakagawa, A., Tanaka, I., Nakahara, K., Shoun, H., Obayashi, E., Nakamura, H., Iizuka, T., and Shiro, Y. (1997) Crystal structure of nitric oxide reductase from denitrifying fungus *Fusarium oxysporum*. *Nat. Struct. Biol. 4*, 827–832.
32. Zerbe, K., Pylypenko, O., Vitali, F., Zhang, W., Rouset, S., Heck, M., Vrijbloed, J. W., Bischoff, D., Bister, B., Sussmuth, R. D., Pelzer, S., Wohlleben, W., Robinson, J. A., and Schlichting, I. (2002) Crystal structure of OxyB, a cytochrome P450 implicated in an oxidative phenol coupling reaction during vancomycin biosynthesis. *J. Biol. Chem. 277*, 47476–47485.
33. Zhao, B., Guengerich, F. P., Bellamine, A., Lamb, D. C., Izumikawa, M., Lei, L., Podust, L. M., Sundaramoorthy, M., Kalaitzis, J. A., Reddy, L. M., Kelly, S. L., Moore, B. S., Stec, D., Voehler, M., Falck, J. R., Shimada, T., and Waterman, M. R. (2005) Binding of two flaviolin substrate molecules, oxidative coupling, and crystal structure of *Streptomyces coelicolor* A3(2) cytochrome P450 158A2. *J. Biol. Chem. 280*, 11599–11607.
34. Yasutake, Y., Imoto, N., Fujii, Y., Fujii, T., Arisawa, A., and Tamura, T. (2007) Crystal structure of cytochrome P450 MoxA from *Nonomuraea recticatena* (CYP105). *Biochem. Biophys. Res. Commun. 361*, 876–882.
35. Cupp-Vickery, J. R., Han, O., Hutchinson, C. R., and Poulos, T. L. (1996) Substrate-assisted catalysis in cytochrome P450eryF. *Nat. Struct. Biol. 3*, 632–637.
36. Podust, L. M., Kim, Y., Arase, M., Neely, B. A., Beck, B. J., Bach, H., Sherman, D. H., Lamb, D. C., Kelly, S. L., and Waterman, M. R. (2003) The 1.92-Å structure of *Streptomyces coelicolor* A3(2) CYP154C1. A new monooxygenase that functionalizes macrolide ring systems. *J. Biol. Chem. 278*, 12214–12221.
37. Nagano, S., Li, H., Shimizu, H., Nishida, C., Ogura, H., Ortiz de Montellano, P. R., and Poulos, T. L. (2003) Crystal structures of epothilone D-bound, epothilone B-bound, and substrate-free forms of cytochrome P450epoK. *J. Biol. Chem. 278*, 44886–44893.
38. Li, H., and Poulos, T. L. (1997) The structure of the cytochrome p450BM-3 haem domain complexed with the fatty acid substrate, palmitoleic acid. *Nat. Struct. Biol. 4*, 140–146.
39. Lee, D. S., Yamada, A., Sugimoto, H., Matsunaga, I., Ogura, H., Ichihara, K., Adachi, S., Park, S. Y., and Shiro, Y. (2003) Substrate recognition and molecular mechanism of fatty acid hydroxylation by cytochrome P450 from *Bacillus subtilis*. Crystallographic, spectroscopic, and mutational studies. *J. Biol. Chem. 278*, 9761–9767.
40. Poulos, T. L. (1995) Cytochrome P450. *Curr. Opin. Struct. Biol. 5*, 767–774.
41. Winn, P. J., Ludemann, S. K., Gauges, R., Lounnas, V., and Wade, R. C. (2002) Comparison of the dynamics of substrate access channels in three cytochrome P450s reveals different opening mechanisms and a novel functional role for a buried arginine. *Proc. Natl. Acad. Sci. U.S.A. 99*, 5361–5366.
42. Tosha, T., Yoshioka, S., Takahashi, S., Ishimori, K., Shimada, H., and Morishima, I. (2003) NMR study on the structural changes of cytochrome P450cam upon the complex formation with putidaredoxin. Functional significance of the putidaredoxin-induced structural changes. *J. Biol. Chem. 278*, 39809–39821.
43. Matsuoka, T., Miyakoshi, S., Tanzawa, K., Nakahara, K., Hosobuchi, M., and Serizawa, N. (1989) Purification and characterization of cytochrome P-450sca from *Streptomyces carbophilus*. ML-236B (compactin) induces a cytochrome P-450sca in *Streptomyces carbophilus* that hydroxylates ML-236B to pravastatin sodium (CS-514), a tissue-selective inhibitor of 3-hydroxy-3-methylglutaryl-coenzyme-A reductase. *Eur. J. Biochem. 184*, 707–713.
44. Taylor, M., Lamb, D. C., Cannell, R., Dawson, M., and Kelly, S. L. (1999) Cytochrome P450105D1 (CYP105D1) from *Streptomyces griseus*: Heterologous expression, activity, and activation effects of multiple xenobiotics. *Biochem. Biophys. Res. Commun. 263*, 838–842.
45. Williams, P. A., Cosme, J., Ward, A., Angove, H. C., Matak Vinkovic, D., and Jhoti, H. (2003) Crystal structure of human cytochrome P450 2C9 with bound warfarin. *Nature 424*, 464–468.

46. Poulos, T. L., Finzel, B. C., and Howard, A. J. (1987) High-resolution crystal structure of cytochrome P450cam. *J. Mol. Biol. 195*, 687–700.
47. Modi, S., Primrose, W. U., Boyle, J. M., Gibson, C. F., Lian, L. Y., and Roberts, G. C. (1995) NMR studies of substrate binding to cytochrome P450 BM3: Comparisons to cytochrome P450 cam. *Biochemistry 34*, 8982–8988.
48. Modi, S., Sutcliffe, M. J., Primrose, W. U., Lian, L. Y., and Roberts, G. C. (1996) The catalytic mechanism of cytochrome P450 BM3 involves a 6 Å movement of the bound substrate on reduction. *Nat. Struct. Biol. 3*, 414–417.
49. Sherman, D. H., Li, S., Yermalitskaya, L. V., Kim, Y., Smith, J. A., Waterman, M. R., and Podust, L. M. (2006) The structural basis for substrate anchoring, active site selectivity, and product formation by P450 PikC from *Streptomyces venezuelae*. *J. Biol. Chem. 281*, 26289–26297.
50. Omura, T., and Ito, A. (1991) Biosynthesis and intracellular sorting of mitochondrial forms of cytochrome P450. *Methods Enzymol. 206*, 75–81.
51. Richardson, T. H., and Johnson, E. F. (1994) Alterations of the regiospecificity of progesterone metabolism by the mutagenesis of two key amino acid residues in rabbit cytochrome P450 2C3v. *J. Biol. Chem. 269*, 23937–23943.
52. Sakaki, T., Kagawa, N., Yamamoto, K., and Inouye, K. (2005) Metabolism of vitamin D_3 by cytochromes P450. *Front. Biosci. 10*, 119–134.

BI7023767